Discrete Phase Shift Design for Practical Large Intelligent Surface Communication

Jindan Xu¹, Student Member, IEEE, Wei Xu^{1,2}, Senior Member, IEEE, and A. Lee Swindlehurst³, Fellow, IEEE

¹National Mobile Communications Research Laboratory, Southeast University, Nanjing 210096, China

²Purple Mountain Laboratories, Nanjing 211111, China

³Center for Pervasive Communications and Computing, University of California, Irvine, CA 92697, USA

Email: {jdxu, wxu}@seu.edu.cn, swindle@uci.edu

Abstract-In this paper, we investigate a downlink channel of a large intelligent surface (LIS) communication system. The LIS is equipped with B-bit discrete phase shifts while base station (BS) exploits low-resolution digital-to-analog converters (DACs). Without the knowledge of channel state information (CSI) related to the LIS, we propose a practical phase shift design method, whose computational complexity increases by 2^B independent of the number of reflecting elements N. A tight lower bound for the asymptotic rate of the user is obtained in closed form. As Nincreases, we observe that the asymptotic rate becomes saturated because both the received signal power and the DAC quantization noise increase. Compared to the optimal continuous phase shift design with perfect CSI, our proposed method asymptotically approaches the ideal benchmark performance for moderate to high values of B. The derived results and observations are verified by simulation results.

Index Terms—large intelligent surface (LIS), low-resolution digital-to-analog converters (DACs), discrete phase shifts, massive multiple-input multiple-output (MIMO)

I. INTRODUCTION

To meet the requirements of ultra-high data rate and massive connections in newly emerging wireless services, large intelligent surface (LIS) has been considered as a potential costeffective technology in the field of wireless communications. The LIS concept can be essentially seen as an extension version of traditional massive multiple-input multiple-output (MIMO) systems [1]. Specifically, an LIS consists of a vast amount of passive reflecting elements whose parameters are reconfigurable with a smart controller. Each of these elements can effectively reflect a phase shifted version of received signal. By adjusting the induced phase shifts in real time, the propagation environment of the reflected signals can be correspondingly changed to conduct beamforming, suppress interference, enhance security, etc. Unlike commonly used amplify-and-forward (AF) relay, LIS performs as a passive array which does not generate new signals. Hence, no additional power consumption is required at LIS.

Recently, some innovative efforts have been devoted to system design and performance analysis for LIS communication systems [2]-[4]. In [2], the total transmit power was minimized

This work was supported in part by the National Natural Science Foundation of China under 61871109 and in part by the Scientific Research Foundation of Graduate School of Southeast University. This work was also supported by Huawei.

by jointly optimizing the transmit beamforming at the access point (AP) and reflect beamforming at the LIS, subject to user's signal-to-interference-and-noise ratio (SINR) constraints. Alternatively, in [3], either energy or spectral efficiency was maximized by jointly optimizing transmit power allocation and coefficients of the LIS. For different propagation scenarios, a tight approximation of the ergodic capacity was formulated in [4]. Moreover, discrete phase shifts are considered in practical systems since ideal continuous phase shifts are not energy efficient and are hard to realize due to hardware limitation [5], [6]. Considering finite-resolution discrete phase shifts, a similar optimization problem as in [2] was further studied in [5]. In [6], it was revealed that even 1-bit phase shifts can achieve significant energy efficiency gains compared to conventional relay-assisted communications.

To the best of our knowledge, most of the existing works assume perfect channel state information (CSI). The equivalent CSI between the AP and the user can be obtained by sending orthogonal pilots. However, the CSI between the AP and the LIS and the CSI between the LIS and the user is in general difficult to achieve because the LIS has limited ability of signal processing. On the other hand, although low-resolution digital-to-analog converters (DACs) have been widely used in massive MIMO communications, their performance in LIS communication systems has not been studied. In this paper, we investigate a downlink channel of an LIS communication system. Finite-resolution discrete phases shifts are exploited at the LIS and low-resolution DACs are adopted at the base station (BS). Without the knowledge of CSI related to the LIS, we propose a practical phase shift design method and derive a tight lower bound for the asymptotic rate of the user. Based on the bound, we analyze the effect of various system parameters on the asymptotic rate.

Notation: \mathbf{A}^T , \mathbf{A}^* , and \mathbf{A}^H represent the transpose, conjugate, and conjugate transpose of \mathbf{A} , respectively. a $\sim \mathcal{CN}(\mathbf{0}, \mathbf{\Sigma})$ denotes a circularly symmetric complex Gaussian vector with zero mean and covariance $\mathbf{\Sigma}$. $\mathcal{W}_m(n, \mathbf{\Sigma})$ denotes an $m \times m$ Wishart matrix with n degrees of freedom and $\mathbf{\Sigma}$ is the covariance matrix of each column. $\mathrm{Tr}(\mathbf{A})$ is the trace of \mathbf{A} . diag(\mathbf{A}) is a matrix that retains only the diagonal entries of \mathbf{A} , while diag{ $a_1, a_2, ..., a_N$ } generates a diagonal matrix with entries $a_1, a_2, ..., a_N$. $\mathcal{U}[a, b]$ represents the uniform distribu-

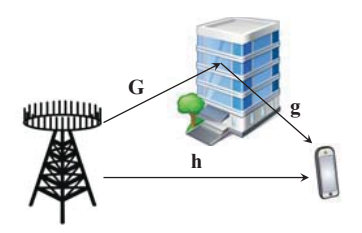


Fig. 1. A downlink LIS communication system.

tion between a and b. $\xrightarrow{\text{a.s.}}$ denotes almost sure convergence.

II. SYSTEM MODEL

A. DAC Quantization Model

Applying Bussang theorem, a linear quantization model has been widely used to characterize the performance of low-resolution DACs [7]. Specifically, the output signal vector of a low-resolution DAC can be decomposed into two uncorrelated parts as [8]

$$Q(\mathbf{x}) = \sqrt{1 - \rho} \mathbf{x} + \mathbf{n}_{q}, \tag{1}$$

where $\mathcal{Q}(\cdot)$ denotes the quantization operation of DACs, \mathbf{x} is a Gaussian input signal vector, $\rho \in (0,1)$ is a distortion factor determined by quantization resolution, and \mathbf{n}_{q} denotes quantization noise yielding

$$\mathbf{C}_{\mathbf{q}} = \mathbb{E}\{\mathbf{n}_{\mathbf{q}}\mathbf{n}_{\mathbf{q}}^{H}\} = \rho \mathbb{E}\left\{\operatorname{diag}\left(\mathbf{x}\mathbf{x}^{H}\right)\right\}.$$
 (2)

Note that the quantization model in (1) has been verified accurate for characterizing commonly used low-resolution DACs [8], [9].

B. Channel Model

We investigate a downlink LIS communication system as illustrated in Fig. 1. The BS is equipped with M antennas and the LIS is equipped with N reflecting elements, serving a single-antenna user. Both the antennas and reflecting elements are arranged in a uniform linear array (ULA). Despite of the direct channel from the BS to the user, the LIS provides a two-hop reflecting channel to improve system performance.

Assuming the line-of-sight (LoS) path between the BS and user is blocked, we model the channel from the BS to the user as Rayleigh fading, denoted by $\mathbf{h} \sim \mathcal{CN}(\mathbf{0}_M, \mathbf{I}_M)$. For the channels from the BS to the LIS and that from the LIS to the user, LoS paths commonly exist and we model these channels as Rician fading. Then, the channel from the BS to the LIS can be expressed as

$$\mathbf{G} = \sqrt{\frac{k_1}{k_1 + 1}} \bar{\mathbf{G}} + \sqrt{\frac{1}{k_1 + 1}} \tilde{\mathbf{G}},\tag{3}$$

where k_1 is the Rician K-factor of \mathbf{G} . $\tilde{\mathbf{G}} \in \mathbb{C}^{N \times M}$ denotes the non-line-of-sight (NLoS) component and the entries of $\tilde{\mathbf{G}}$ follow i.i.d. complex Gaussian distribution with zero mean and unit variance. $\bar{\mathbf{G}} \in \mathbb{C}^{N \times M}$ denotes the LoS component and it can be expressed as

$$\bar{\mathbf{G}} = \mathbf{g}_R \mathbf{g}_P^H, \tag{4}$$

where $\mathbf{g}_B \in \mathbb{C}^{M \times 1}$ and $\mathbf{g}_R \in \mathbb{C}^{N \times 1}$ denote the antenna array response vectors at the BS and LIS respectively. More specifically, we have

$$\mathbf{g}_{B} = \left[1, e^{-j2\pi \frac{d}{\lambda}\cos\phi}, ..., e^{-j2\pi(M-1)\frac{d}{\lambda}\cos\phi}\right]^{T}, \quad (5)$$

$$\mathbf{g}_{R} = \left[1, e^{-j2\pi \frac{d}{\lambda}\cos\varphi}, ..., e^{-j2\pi(N-1)\frac{d}{\lambda}\cos\varphi}\right]^{T}, \quad (6)$$

where $\phi \sim \mathcal{U}[0,\pi]$ is the angle of departure (AoD) of the ULA at the BS while $\varphi \sim \mathcal{U}[0,\pi]$ is the angle of arrival (AoA) at the LIS. Similarly, the channel vector from the LIS to the user is given as

$$\mathbf{g} = \sqrt{\frac{k_2}{k_2 + 1}}\bar{\mathbf{g}} + \sqrt{\frac{1}{k_2 + 1}}\tilde{\mathbf{g}},$$
 (7)

where k_2 is the Rician K-factor of \mathbf{g} , $\tilde{\mathbf{g}} \sim \mathcal{CN}(\mathbf{0}_N, \mathbf{I}_N)$ denotes the NLoS component, and $\bar{\mathbf{g}} \in \mathbb{C}^{N \times 1}$ denotes the LoS component expressed as

$$\bar{\mathbf{g}} = \left[1, e^{-j2\pi \frac{d}{\lambda}\cos\psi}, ..., e^{-j2\pi(N-1)\frac{d}{\lambda}\cos\psi}\right]^T, \quad (8)$$

where $\psi \sim \mathcal{U}[0,\pi]$ is the AoD of the reflected signal at the LIS

At the LIS, each element first combines all the received multi-path signals and then reflected these signals with a certain phase shift. Let

$$\mathbf{\Theta} = \operatorname{diag}\{e^{j\theta_1}, e^{j\theta_2}, ..., e^{j\theta_N}\}$$
(9)

denote the phase shift matrix at the LIS, where θ_i is the phase shift of the ith reflecting element. At the BS, the transmit signal s is precoded by a normalized vector $\mathbf{w} \in \mathbb{C}^{M \times 1}$. We assume that $\mathbb{E}\left\{|s|^2\right\} = 1$ and $\|\mathbf{w}\|^2 = 1$. Applying the DAC quantization model in (1), the received signal at the user can be expressed as

$$y = (\mathbf{g}^{H} \mathbf{\Theta} \mathbf{G} + \mathbf{h}^{H}) \mathcal{Q} \left(\sqrt{P} \mathbf{w} s \right) + n$$

$$= \sqrt{(1 - \rho)P} \left(\mathbf{g}^{H} \mathbf{\Theta} \mathbf{G} + \mathbf{h}^{H} \right) \mathbf{w} s + \left(\mathbf{g}^{H} \mathbf{\Theta} \mathbf{G} + \mathbf{h}^{H} \right) \mathbf{n}_{q} + n,$$
(10)

where $n \sim \mathcal{CN}(0, \sigma_n^2)$ denotes the thermal noise with power σ_n^2 . Assuming that the equivalent channel, $\mathbf{g}^H \mathbf{\Theta} \mathbf{G} + \mathbf{h}^H$, is known to the BS, we adopt an maximal-ratio-transmission (MRT) precoder as

$$\mathbf{w} = \frac{\left(\mathbf{g}^H \mathbf{\Theta} \mathbf{G} + \mathbf{h}^H\right)^H}{\|\mathbf{g}^H \mathbf{\Theta} \mathbf{G} + \mathbf{h}^H\|}.$$
 (11)

By substituting (11) into (10), the signal-to-quantization-andnoise ratio (SQNR) of the received signal is obtained as

$$\gamma_{\mathbf{u}} = \frac{(1 - \rho)P \left\| \mathbf{g}^{H} \mathbf{\Theta} \mathbf{G} + \mathbf{h}^{H} \right\|^{2}}{(\mathbf{g}^{H} \mathbf{\Theta} \mathbf{G} + \mathbf{h}^{H}) \mathbf{C}_{\mathbf{q}} (\mathbf{g}^{H} \mathbf{\Theta} \mathbf{G} + \mathbf{h}^{H})^{H} + \sigma_{n}^{2}}, \quad (12)$$

where

$$\mathbf{C}_{\mathbf{g}} = \rho P \operatorname{diag}\left(\mathbf{w}\mathbf{w}^{H}\right). \tag{13}$$

Considering a large number of reflecting elements, the asymp-

totic SQNR is given in the following lemma.

Lemma 1. As $M, N \xrightarrow{a.s.} \infty$, the SQNR of the user almost surely converges to

$$\gamma = \frac{(1 - \rho)P\left(\alpha \left\|\bar{\mathbf{g}}^H \mathbf{\Theta} \bar{\mathbf{G}}\right\|^2 + \beta M N + M\right)}{\frac{\rho P}{M}\left(\alpha \left\|\bar{\mathbf{g}}^H \mathbf{\Theta} \bar{\mathbf{G}}\right\|^2 + \beta M N + M\right) + \sigma_n^2},$$
 (14)

where we define

$$\alpha \triangleq \frac{k_1 k_2}{(k_1 + 1)(k_2 + 1)},\tag{15}$$

$$\beta \triangleq \frac{k_1 + k_2 + 1}{(k_1 + 1)(k_2 + 1)}. (16)$$

Proof: See Appendix A.

By applying Shannon's formula, the asymptotic rate of the user is obtained as

$$R = \log_{2} (1 + \gamma)$$

$$= \log_{2} \left(1 + \frac{(1 - \rho)P\left(\alpha \|\bar{\mathbf{g}}^{H}\boldsymbol{\Theta}\bar{\mathbf{G}}\|^{2} + \beta MN + M\right)}{\frac{\rho P}{M}\left(\alpha \|\bar{\mathbf{g}}^{H}\boldsymbol{\Theta}\bar{\mathbf{G}}\|^{2} + \beta MN + M\right) + \sigma_{n}^{2}} \right)$$

$$= \log_{2} \left(1 + \frac{(1 - \rho)M}{\rho} - \frac{(1 - \rho)M\sigma_{n}^{2}}{\frac{\rho^{2}P}{M}\left(\alpha \|\bar{\mathbf{g}}^{H}\boldsymbol{\Theta}\bar{\mathbf{G}}\|^{2} + \beta MN + M\right) + \rho\sigma_{n}^{2}} \right). \tag{17}$$

Remark 1. From (17), we observe that the asymptotic user rate increases with M, N, and P. Lower DAC resolution leads to larger distortion parameter ρ , which inevitably causes significant degradation in R. The impact of N phase shifts at the LIS relies on the term $\|\bar{\mathbf{g}}^H \mathbf{\Theta} \bar{\mathbf{G}}\|^2$, requiring further discussion in the following.

III. PHASE SHIFT DESIGN AT LIS

In this section, we propose a discrete phase shift design method for Θ . Before that, we introduce the optimal continuous phase shift design with perfect CSI, which achieves an ideal benchmark for the rate performance.

A. Optimal Continuous Phase Shift Design

Using (17), the optimal phase shift design satisfies

$$\mathbf{\Theta}^* = \arg \max_{\mathbf{\Theta}} R = \arg \max_{\mathbf{\Theta}} \|\bar{\mathbf{g}}^H \mathbf{\Theta} \bar{\mathbf{G}}\|^2$$
 (18)

This optimization problem is similar to that in [4, Eq. (23)], although low-resolution DACs are used in this work. Given g_R and $\bar{\mathbf{g}}$, i.e., φ and ψ , the solution to (18) has been obtained in [4, Eq. (27)]. We conclude the solution in the following lemma.

Lemma 2. Given φ and ψ , the optimal Θ^* is obtained as

$$\mathbf{\Theta}^* = \text{diag}\{1, e^{j\theta}, \dots, e^{j(N-1)\theta}\},\tag{19}$$

where

$$\theta = 2\pi \frac{d}{\lambda} (\cos \varphi - \cos \psi). \tag{20}$$

Applying Lemma 2 and using (4) and (8), the maximal value of $\|\bar{\mathbf{g}}^H \boldsymbol{\Theta} \bar{\mathbf{G}}\|^2$ equals MN^2 . Substituting this into (17), the optimal asymptotic user rate is

$$R^* = \log_2 \left(1 + \frac{(1 - \rho)M}{\rho} - \frac{(1 - \rho)M\sigma_n^2}{\rho^2 P(\alpha N^2 + \beta N + 1) + \rho\sigma_n^2} \right). \tag{21}$$

Remark 2. From (21), we have $R^* \to \log_2\left(1 + \frac{(1-\rho)M}{\rho}\right)$ for $N \to \infty$. This implies that the asymptotic rate becomes saturated instead of increasing infinitely as the number of reflecting elements increases. This is because both the DAC quantization noise and the received signal power simultaneously increase with N. In an LIS communication system, extremely large number of reflecting elements are not necessary when low-resolution DACs are adopted. On the other hand, increasing M, i.e., the number of antennas at the BS, can effectively improve the user rate.

As revealed in Lemma 2, the optimal continuous phase shift design requires the AOA and AOD of the reflecting element array at the LIS. However, it is in general difficult to achieve the information of \mathbf{g}_R and $\bar{\mathbf{g}}$ because the LIS performs as a passive scatter. On the other hand, ideal continuous phase shifts cause high hardware and power consumptions, especially for a large number of reflecting elements. For these reasons, we propose a discrete phase shift design method without the knowledge of g_R and \bar{g} in the following.

B. Discrete Phase Shift Design

We first introduce a practical approach to determine the discrete phase shifts at the LIS, which is similar to the AOA estimation procedure in [10]. In each coherence interval, the BS broadcasts a frequency tone $x = \cos 2\pi ft$ from an arbitrary antenna. The LIS reflects the received signal to the user, and the received signal at the user is

$$y' = \mathbf{g}^H \mathbf{\Theta} \mathbf{G} x + \mathbf{h}^H x + n', \tag{22}$$

where $n' \sim \mathcal{CN}(0, \sigma_n^2)$ denotes the thermal noise. Considering discrete phase shifts constrained by a limited quantization resolution B, angles of each diagonal element of Θ is chosen from a codebook:

$$\Omega = \{0, 2\delta, ..., (2^{B+1} - 2) \delta\}, \tag{23}$$

where $\delta \triangleq \frac{\pi}{2^B}$. According to (18), the estimated optimal Θ can be obtained by

$$\widehat{\boldsymbol{\Theta}} = \arg \max_{\substack{\boldsymbol{\Theta} = \operatorname{diag}\{e^{j\theta_{1}}, e^{j\theta_{2}}, \dots, e^{j\theta_{N}}\}, \\ \boldsymbol{\theta}_{i} \in \boldsymbol{\Omega}, \ \forall i \in \{1, 2, \dots, N\}}} \left\| \overline{\mathbf{g}}^{H} \boldsymbol{\Theta} \overline{\mathbf{G}} \right\|^{2}$$

$$= \arg \max_{\substack{\boldsymbol{\Theta} = \operatorname{diag}\{e^{j\theta_{1}}, e^{j\theta_{2}}, \dots, e^{j\theta_{N}}\}, \\ \boldsymbol{\theta}_{i} \in \boldsymbol{\Omega}, \ \forall i \in \{1, 2, \dots, N\}}} |y'|^{2} \qquad (24)$$

$$\approx \arg \max_{\substack{\boldsymbol{\Theta} = \operatorname{diag}\{1, e^{j\theta}, \dots, e^{j(N-1)\theta}\}, \\ \boldsymbol{\theta} \in \boldsymbol{\Omega}}} |y'|^{2}, \qquad (25)$$

$$\approx \arg \max_{\boldsymbol{\Theta} = \operatorname{diag}\{1, e^{j\theta}, \dots, e^{j(N-1)\theta}\}, \ |y'|^2, \tag{25}$$

where (24) uses (22). Note that the power of terms $\mathbf{h}^H x$ and n' have constant expectations and thus their effect can be neglected. In this way, the optimal $\boldsymbol{\Theta}$ can be obtained by maximizing the power of the received signal at the user. Further in (25), in order to reduce the complexity of exhausted search for θ_i , $\forall i \in \{1, 2, ..., N\}$, from Ω with large N, we utilize the constraint in Lemma 2 that the phases of diagonal elements of the optimal $\boldsymbol{\Theta}$ form an arithmetic sequence. In this way, the searching set size of candidate $\hat{\boldsymbol{\Theta}}$ reduces from 2^{NB} to 2^B .

Let

$$\widehat{\mathbf{\Theta}} = \operatorname{diag}\{1, e^{j\hat{\theta}}, \dots, e^{j(N-1)\hat{\theta}}\},\tag{26}$$

denote the obtained phase matrix from (25) and

$$\Delta \theta \triangleq \hat{\theta} - \theta, \tag{27}$$

denote the phase quantization error where θ is given in (20). We assume that $\Delta\theta \in [-\delta, \delta]$. For the proposed discrete phase shift design method, a lower bound for the asymptotic rate of the user is given in the following theorem.

Theorem 1. Using $\widehat{\Theta}$ in (25) at the LIS and considering low-resolution DACs at the BS, a lower bound for the asymptotic rate of the user is obtained as

$$\hat{R}_{L} = \log_{2} \left(1 + \frac{(1-\rho)M}{\rho} - \frac{(1-\rho)M\sigma_{n}^{2}}{\rho^{2}P\left[\alpha(N-1)^{2}\operatorname{Sa}^{2}\left(\frac{N-1}{2}\delta\right) + \beta N + 1\right] + \rho\sigma_{n}^{2}} \right),$$
(28)

where $Sa(x) \triangleq \frac{\sin x}{x}$.

Proof: The lower bound in (28) is obtained by substituting $\left\|\bar{\mathbf{g}}^H\widehat{\boldsymbol{\Theta}}\bar{\mathbf{G}}\right\|^2 \geq M(N-1)^2\mathrm{Sa}^2\left(\frac{N-1}{2}\delta\right)$ into (17), where we use the fact that $|\sin(x)| \leq |x|$ for $-\frac{\pi}{2} \leq x \leq \frac{\pi}{2}$ and the properties of sampling function $\mathrm{Sa}(x)$. Due to the page limit, we leave out the proof details.

Remark 3. By comparing \hat{R}_L in (28) to R^* in (17), we observe that the distortion of user rate caused by discrete phase shifts relies on the term $(N-1)^2\mathrm{Sa}^2\left(\frac{N-1}{2}\delta\right)$, which replaces the term N^2 in R^* . The phase interval δ decreases with resolution B increasing, leading to a higher asymptotic rate. For moderate to high values of B, we have $\mathrm{Sa}^2\left(\frac{N-1}{2}\delta\right)\approx 1$ and thus \hat{R}_L approaches R^* in this case.

IV. NUMERICAL RESULTS

In this section, we verify the derived lower rate bound in Theorem 1 for the proposed discrete phase shift design method, compared to the optimal continuous phase shift design.

Fig. 2 shows the user rate versus the number of antennas M. $\frac{P}{\sigma_n^2}$ denotes signal-to-noise ratio of the system and 3-bit DACs are exploited at the BS. Dotted markers correspond to numerical results while solid lines correspond to the analytical result in (28). Obviously, the derived lower bound for the

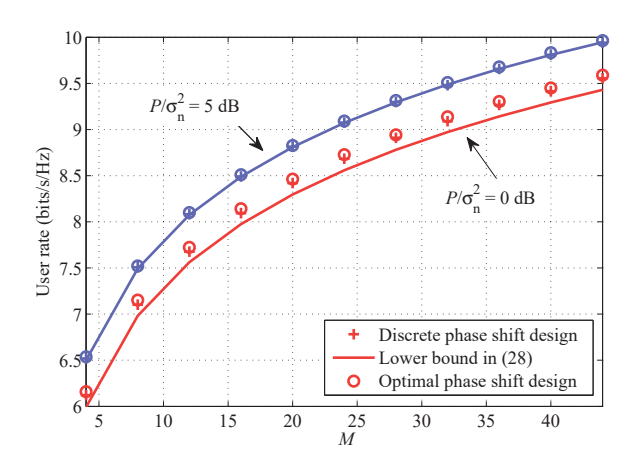


Fig. 2. User rate and the derived lower bound versus M using 3-bit DACs $(B=4,\ N=8,\ {\rm and}\ k_1=k_2=10).$

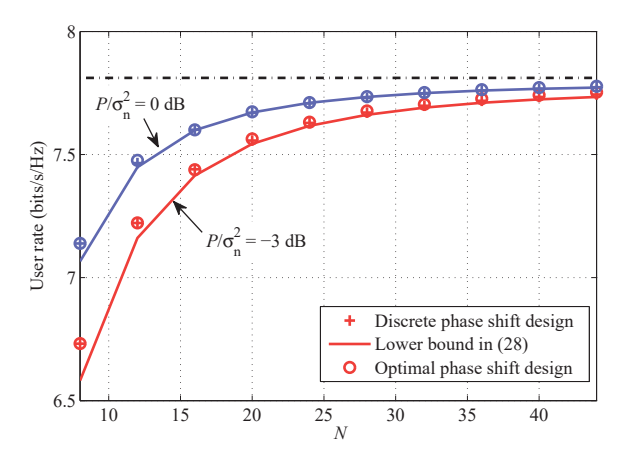


Fig. 3. User rate and the derived lower bound versus N using 3-bit DACs $(B=6,\ M=8,\ {\rm and}\ k_1=k_2=10).$

user rate is verified accurate. The proposed practical phase shift design method, which uses 4-bit discrete phase shifts, achieves nearly the same rate as the optimal one. In addition, we observe that the user rate monotonically increases with M because more antennas can achieve larger diversity gain. This implies that adding antennas at the BS can significantly improve the user rate.

Fig. 3 shows the user rate versus the number of reflecting elements N using 3-bit DACs. Unlike in Fig. 2, the user rate becomes saturated when N increases, as indicated in Remark 2. The dashed line in the figure denote the asymptotic upper benchmark of the user rate, i.e., $R^*, \hat{R}_L \rightarrow \log_2\left(1+\frac{(1-\rho)M}{\rho}\right)$ for $N\rightarrow\infty$. According to the DAC quantization model in (1), both the received power of signals and quantization noise increases with N. Given a fixed thermal noise power, the SQNR first increases with N, which results in an increasing user rate. As N continues increasing, the power of thermal noise becomes neglectable compared to the power of received signals and quantized noise. Hence, the SQNR

saturates to a constant independent of N, leading to a saturated user rate.

V. CONCLUSIONS

In this work, we investigated an LIS communication system employing discrete phase shifts and low-resolution DACs. Without the knowledge of CSI related to the LIS, we propose a practical phase shift design method. Moreover, a lower bound for the asymptotic rate of the user is obtained. For moderate to high phase resolutions, we observe that our proposed method asymptotically approaches the ideal benchmark performance of the optimal continuous phase shift design with perfect CSI.

APPENDIX A PROOF OF LEMMA 1

According to (11), we have

$$\mathbf{w}\mathbf{w}^{H} = \frac{\left(\mathbf{g}^{H}\boldsymbol{\Theta}\mathbf{G} + \mathbf{h}^{H}\right)^{H} \left(\mathbf{g}^{H}\boldsymbol{\Theta}\mathbf{G} + \mathbf{h}^{H}\right)}{\|\mathbf{g}^{H}\boldsymbol{\Theta}\mathbf{G} + \mathbf{h}^{H}\|^{2}}$$
(29)

Due to the strong law of large numbers for large M, $\operatorname{diag}\left(\mathbf{w}\mathbf{w}^{H}\right)$ in (13) almost surely converges to a scaled identity matrix. Along with $\operatorname{Tr}\left\{\mathbf{w}\mathbf{w}^{H}\right\} = \|\mathbf{w}\|^{2} = 1$, we have $\operatorname{diag}\left(\mathbf{w}\mathbf{w}^{H}\right) \xrightarrow{a.s.} \frac{1}{M}\mathbf{I}_{M}$. Substituting this into (13), it yields

$$\mathbf{C}_{\mathbf{q}} \xrightarrow{a.s.} \frac{\rho P}{M} \mathbf{I}_{M}.$$
 (30)

On the other hand, by substituting (3) and (7), we have

$$\|\mathbf{g}^{H}\boldsymbol{\Theta}\mathbf{G}+\mathbf{h}^{H}\|$$

$$= \left\|\sqrt{\frac{1}{(k_{1}+1)(k_{2}+1)}}\left(\sqrt{k_{1}k_{2}}\bar{\mathbf{g}}^{H}\boldsymbol{\Theta}\bar{\mathbf{G}} + \sqrt{k_{1}}\tilde{\mathbf{g}}^{H}\boldsymbol{\Theta}\bar{\mathbf{G}}\right) + \mathbf{h}^{H}\right\|^{2}$$

$$+ \sqrt{k_{2}}\bar{\mathbf{g}}^{H}\boldsymbol{\Theta}\tilde{\mathbf{G}} + \tilde{\mathbf{g}}^{H}\boldsymbol{\Theta}\tilde{\mathbf{G}}\right) + \mathbf{h}^{H}\|^{2}$$

$$\xrightarrow{a.s.} \frac{1}{(k_{1}+1)(k_{2}+1)}\left(k_{1}k_{2}\|\bar{\mathbf{g}}^{H}\boldsymbol{\Theta}\bar{\mathbf{G}}\|^{2} + k_{1}\|\tilde{\mathbf{g}}^{H}\boldsymbol{\Theta}\bar{\mathbf{G}}\|^{2} + k_{2}\|\bar{\mathbf{g}}^{H}\boldsymbol{\Theta}\tilde{\mathbf{G}}\|^{2} + \|\tilde{\mathbf{g}}^{H}\boldsymbol{\Theta}\tilde{\mathbf{G}}\|^{2}\right) + \|\mathbf{h}^{H}\|^{2}$$

$$+ k_{2}\|\bar{\mathbf{g}}^{H}\boldsymbol{\Theta}\tilde{\mathbf{G}}\|^{2} + \|\tilde{\mathbf{g}}^{H}\boldsymbol{\Theta}\tilde{\mathbf{G}}\|^{2}\right) + \|\mathbf{h}^{H}\|^{2}$$

$$\xrightarrow{a.s.} \frac{1}{(k_{1}+1)(k_{2}+1)}\left(k_{1}k_{2}\|\bar{\mathbf{g}}^{H}\boldsymbol{\Theta}\bar{\mathbf{G}}\|^{2} + k_{1}MN\right)$$

$$(31)$$

where (31) uses the assumption that $\tilde{\mathbf{g}}$, $\tilde{\mathbf{G}}$, and \mathbf{h} are independent with each other and have zero means, and (32) uses the following results

 $+k_2MN+MN)+M,$

$$\|\tilde{\mathbf{g}}^{H}\boldsymbol{\Theta}\bar{\mathbf{G}}\|^{2} = \operatorname{tr}\left\{\tilde{\mathbf{g}}^{H}\boldsymbol{\Theta}\bar{\mathbf{G}}\bar{\mathbf{G}}^{H}\boldsymbol{\Theta}^{H}\tilde{\mathbf{g}}\right\}$$

$$= \operatorname{tr}\left\{\bar{\mathbf{G}}^{H}\boldsymbol{\Theta}^{H}\tilde{\mathbf{g}}\tilde{\mathbf{g}}^{H}\boldsymbol{\Theta}\bar{\mathbf{G}}\right\}$$

$$\xrightarrow{a.s.} \operatorname{tr}\left\{N\mathbf{g}_{B}\mathbf{g}_{B}^{H}\right\}$$

$$= MN. \tag{34}$$

$$\left\| \bar{\mathbf{g}}^{H} \boldsymbol{\Theta} \tilde{\mathbf{G}} \right\|^{2} = \bar{\mathbf{g}}^{H} \boldsymbol{\Theta} \tilde{\mathbf{G}} \tilde{\mathbf{G}}^{H} \boldsymbol{\Theta}^{H} \bar{\mathbf{g}}$$

$$\xrightarrow{a.s.} M \bar{\mathbf{g}}^{H} \boldsymbol{\Theta} \boldsymbol{\Theta}^{H} \bar{\mathbf{g}}$$

$$= MN. \tag{35}$$

$$\begin{split} \left\| \tilde{\mathbf{g}}^{H} \boldsymbol{\Theta} \tilde{\mathbf{G}} \right\|^{2} &= \tilde{\mathbf{g}}^{H} \boldsymbol{\Theta} \tilde{\mathbf{G}} \tilde{\mathbf{G}}^{H} \boldsymbol{\Theta}^{H} \tilde{\mathbf{g}} \\ &\xrightarrow{a.s.} M \tilde{\mathbf{g}}^{H} \boldsymbol{\Theta} \boldsymbol{\Theta}^{H} \tilde{\mathbf{g}} \\ &= M \tilde{\mathbf{g}}^{H} \tilde{\mathbf{g}} \\ &\xrightarrow{a.s.} MN, \end{split} \tag{38}$$

$$\left\| \mathbf{h}^{H} \right\|^{2} = \mathbf{h}^{H} \mathbf{h}$$

$$\xrightarrow{a.s.} M.$$
(39)

where (33) uses the property of the complex Wishart matrix $\bar{\mathbf{G}}^H \boldsymbol{\Theta}^H \tilde{\mathbf{g}} \tilde{\mathbf{g}}^H \boldsymbol{\Theta} \bar{\mathbf{G}} \sim \mathcal{W}_M \left(1, N \mathbf{g}_B \mathbf{g}_B^H \right) [11], (35)$ and (37) comes from $\frac{1}{M} \tilde{\mathbf{G}} \tilde{\mathbf{G}}^H \xrightarrow{a.s.} \mathbf{I}_N$, (38) uses $\frac{1}{N} \tilde{\mathbf{g}}^H \tilde{\mathbf{g}} \xrightarrow{a.s.} 1$, and (39) utilizes $\frac{1}{M} \mathbf{h}^H \mathbf{h} \xrightarrow{a.s.} 1$, due to the strong law of large numbers for large M and N.

Since convergence is preserved for continuous functions according to the Continuous Mapping Theorem [12], the asymptotic SQNR in (14) is obtained by substituting (30) and (32) into (12) and using the definitions in (15) and (16).

REFERENCES

- [1] S. Hu, F. Rusek, and O. Edfors, "Byond massive MIMO: The potential of data transmission with large intelligent surfaces," *IEEE Trans. Sig. Process.*, vol. 66, no. 10, pp. 2746–2758, May 2018.
- [2] Q. Wu and R. Zhang, "Intelligent reflecting surface enhanced wireless network via joint active and passive beamforming," *submitted* to *IEEE Trans. Wireless Commun.*, 2018, [Online] Available: https://arxiv.org/abs/1810.03961.
- [3] C. Huang, A. Zappone, G. C. Alexandropoulos, M. Debbah, and C. Yuen, "Large intelligent surfaces for energy efficiency in wireless communication," *submitted to IEEE Trans. Wireless Commun.*, 2018, [Online] Available: https://arxiv.org/abs/1810.06934.
- [4] Y. Han, W. Tang, S. Jin, C. Wen, and X. Ma, "Large intelligent surfaceassisted wireless communication exploiting statistical CSI," Dec. 2018, [Online]. Available: https://arxiv.org/pdf/1812.05429
- [5] Q. Wu and R. Zhang, "Beamforming optimization for intelligent reflecting surface with discrete phase shifts," in *Proc. IICASSP*, Brighton, UK, May 2019.
- [6] C. Huang, G. C. Alexandropoulos, A. Zappone, M. Debbah, and C. Yuen, "Energy efficient multi-user MISO communication using low resolution large intelligent surfaces,// in *Proc. GLOBECOM*, Abu Dhabi, UAE, Dec. 2018.
- [7] J. Xu, W. Xu, J. Zhu, D. W. K. Ng, and A. L. Swindlehurst, "Secure massive MIMO communication with low-resolution DACs," *IEEE Trans. Commun.*, vol. 67, no. 5, pp. 3265–3278, May. 2019.
- [8] J. Xu, W. Xu, and F. Gong, "On performance of quantized transceiver in multiuser massive MIMO downlinks," *IEEE Wireless Commun. Lett.*, vol. 6, no. 5, pp. 562–565, Jun. 2017.
- [9] S. Jacobsson, G. Durisi, M. Coldrey, T. Coldstein, and C. Studer, "Quantized precoding for massive MU-MIMO", *IEEE Trans. Commun.*, vol. 65, no. 11, pp. 4670–4684, Jul. 2017.
- [10] J. Xu, W. Xu, H. Zhang, G. Y. Li, and X. You, "Performance analysis of multi-cell millimeter wave massive MIMO networks with low-precision ADCs," *IEEE Trans. Commun.*, vol. 67, no. 1, pp. 302–317, Jan. 2019.
- [11] A. M. Tulino and S. Verdu, Random Matrix Theory and Wireless Communications, Hanover, MA: Now Publishers Inc., 2004.
- [12] P. Billingsley, Convergence of Probability Measures, Hoboken, YK: John Wiley & Sons, 1969.

(32)